JCB Journal of Cell Biology

REPORT

Transmembrane phospholipid translocation mediated by Atg9 is involved in autophagosome formation

Minami Orii[1]*, Takuma Tsuji[2]*, Yuta Ogasawara[2], and Toyoshi Fujimoto[2]

The mechanism of isolation membrane formation in autophagy is receiving intensive study. We recently found that Atg9 translocates phospholipids across liposomal membranes and proposed that this functionality plays an essential role in the expansion of isolation membranes. The distribution of phosphatidylinositol 3-phosphate in both leaflets of yeast autophagosomal membranes supports this proposal, but if Atg9-mediated lipid transport is crucial, symmetrical distribution in autophagosomes should be found broadly for other phospholipids. To test this idea, we analyzed the distributions of phosphatidylcholine, phosphatidylserine, and phosphatidylinositol 4-phosphate by freeze-fracture electron microscopy. We found that all these phospholipids are distributed with comparable densities in the two leaflets of autophagosomes and autophagic bodies. Moreover, de novo–synthesized phosphatidylcholine is incorporated into autophagosomes preferentially and shows symmetrical distribution in autophagosomes within 30 min after synthesis, whereas this symmetrical distribution is compromised in yeast expressing an Atg9 mutant. These results indicate that transbilayer phospholipid movement that is mediated by Atg9 is involved in the biogenesis of autophagosomes.

Introduction

Macroautophagy (hereafter referred to as autophagy) is a conserved catabolic pathway in eukaryotes. In the budding yeast *Saccharomyces cerevisiae*, autophagy initiates at the preautophagosomal structure by formation of the isolation membrane (phagophore), followed by its maturation to the double-membrane autophagosome, which eventually fuses with the vacuole (yeast lysosome), leading to degradation of engulfed cargoes (Bento et al., 2016; Mizushima et al., 2011; Nakatogawa, 2020). The proteins that are necessary for the autophagic process have been analyzed extensively, and the molecular mechanisms underlying the various steps are beginning to emerge. Nevertheless, there are still many unanswered questions, one of which is how the phospholipids for isolation membrane/autophagosome formation are supplied.

A recent study has shown that de novo phospholipid synthesis driven by acyl-CoA synthetase, Faa1, is critical for the expansion of isolation membranes (Schütter et al., 2020). Phospholipids synthesized through this process are thought to be supplied from the ER exit site (ERES) to isolation membranes via nonvesicular transport mediated by Atg2 (Graef et al., 2013; Kishi-Itakura et al., 2014; Suzuki et al., 2013; Velikkakath et al., 2012). Atg2 and its mammalian homologue, ATG2, have a hydrophobic cavity that can accommodate many phospholipid molecules, tether two liposomes, and mediate phospholipid transport between liposomes (Chowdhury et al., 2018; Kotani et al., 2018; Maeda et al., 2019; Osawa et al., 2019; Valverde et al., 2019). Thus, it has been thought that Atg2 binds to the ERES on one end and the isolation membrane on the other end, thereby supplying phospholipids for the isolation membrane formation (Osawa et al., 2019; Valverde et al., 2019).

The Atg2-dependent process, however, can only transport phospholipids to the cytoplasmic leaflet of isolation membranes. For isolation membranes to expand, phospholipids need to be provided to the noncytoplasmic leaflet as well. In this context, we recently showed that yeast Atg9, the only transmembrane protein in the core Atg proteins, translocates phospholipids across liposome membranes, suggesting that Atg9 may function as a phospholipid scramblase in the isolation membrane (Matoba et al., 2020). Distribution of phosphatidylinositol 3-phosphate (PtdIns(3)P) in both leaflets of yeast autophagosomal membranes (Cheng et al., 2014) is consistent with this putative Atg9 functionality, but PtdIns(3)P is a minor phospholipid and the transbilayer movement of this lipid alone would not be sufficient for isolation membrane expansion.

[1]Department of Anatomy and Molecular Cell Biology, Nagoya University Graduate School of Medicine, Nagoya, Japan; [2]Laboratory of Molecular Cell Biology, Research Institute for Diseases of Old Age, Juntendo University Graduate School of Medicine, Tokyo, Japan.

*M. Orii and T. Tsuji contributed equally to this paper; Correspondence to Toyoshi Fujimoto: t.fujimoto.xl@juntendo.ac.jp; M. Orii's present address is Department of Biochemistry, Showa University School of Medicine, Tokyo, Japan.

In the present study, we explored whether phospholipids other than PtdIns(3)P are also distributed in both leaflets of the isolation membrane/autophagosome. Specifically, we examined two major phospholipids, phosphatidylcholine (PtdCho) and phosphatidylserine (PtdSer), as well as phosphatidylinositol 4-phosphate (PtdIns(4)P), by quick-freeze and freeze-fracture replica labeling EM (QF-FRL; Fig. S1 A), which revealed lipid distribution in individual membrane leaflets (Tsuji et al., 2019). We also examined how de novo–synthesized PtdCho is incorporated into autophagic membranes by combining QF-FRL and metabolic labeling with a clickable choline analogue (Iyoshi et al., 2014). We found that autophagosomes and autophagic bodies are the only membranes in which all these phospholipids show symmetrical distribution across the lipid bilayer. Moreover, de novo–synthesized PtdCho was found to be distributed in both leaflets of autophagosomal membranes within 30 min after synthesis without dispersing to the ER and other cellular membranes. Incorporation of de novo–synthesized PtdCho into the noncytoplasmic leaflet of autophagosomal membranes was compromised in yeast expressing an Atg9 mutant that was decreased in the phospholipid translocation activity in liposomes (Matoba et al., 2020). Our results indicate that highly efficient transbilayer phospholipid transport that is mediated by Atg9 occurs in isolated membranes/autophagosomes.

Results and discussion

Symmetrical distribution of PtdCho and PtdSer in autophagic membranes

PtdCho is a major phospholipid in the yeast autophagosomal membrane (Schütter et al., 2020). We previously clarified the distribution patterns of PtdCho in the budding yeast *S. cerevisiae* by metabolic labeling with the clickable choline analogue propargylcholine and click reaction in freeze-fracture replicas (Fig. S1 B; Iyoshi et al., 2014). We found that PtdCho is distributed symmetrically across the phospholipid bilayer of all organelles, but not in the plasma membrane (Iyoshi et al., 2014). In the present study, using the same methodology, we analyzed PtdCho in autophagic membranes. Yeast was cultured overnight in synthetic complete (SC) medium containing 1 mM propargylcholine to label PtdCho in all cellular membranes, and then transferred to nitrogen- and carbon-deficient synthetic medium (S(–NC)) supplemented with 1 mM propargylcholine for 4 h. (In this and subsequent experiments, vacuolar proteolysis was blocked by adding 1 mM phenylmethylsulphonyl fluoride or by using *pep4Δ* cells to observe autophagic bodies.) This technique revealed intense PtdCho labeling in comparable densities in the cytoplasmic and noncytoplasmic leaflets, in both the outer and inner autophagosomal membranes (Fig. 1, A and B). Autophagic bodies that were derived from the inner autophagosomal membrane were also labeled similarly in the two leaflets (Fig. 1 C). The specificity of the labeling was confirmed by omitting propargylcholine from the culture medium or by using the click reaction mixture without biotin-azide (Iyoshi et al., 2014).

For PtdSer, endogenous lipids were labeled by using the evectin-2 pleckstrin-homology (PH) domain (Tsuji et al., 2019). In yeast in a logarithmic growth phase, PtdSer is distributed in both leaflets of most organelles, whereas it is confined to the cytoplasmic leaflet in the vacuole and the plasma membrane (Tsuji et al., 2019). When autophagy was induced by culturing in S(–NC) for 4 h, PtdSer was intensely labeled in both the cytoplasmic and noncytoplasmic leaflets of autophagosomes (Fig. 2 A). Autophagic bodies were also labeled in both leaflets (Fig. 2 B). Furthermore, after autophagic induction, the lumenal leaflet of vacuoles showed a significant increase in PtdSer (Fig. 2 C), which is thought to be caused by the fusion of outer autophagosomal membranes to vacuoles. The labeling was negligible when a PH domain mutant lacking the affinity to PtdSer was used, confirming its specificity (Tsuji et al., 2019). The overall labeling density of PtdSer is comparable to that of PtdCho, but this does not indicate that the actual concentrations of PtdSer and PtdCho are similar, because the labeling efficiency is different for each phospholipid.

The results showed that PtdCho and PtdSer are present in both leaflets of autophagosomes. This distribution could be generated if isolation membranes/autophagosomes were to expand by the fusion of vesicles derived from other organelles with symmetrical PtdCho/PtdSer distributions. Atg9 vesicles, which contain both PtdCho and PtdSer (Sawa-Makarska et al., 2020), are involved in isolation membrane/autophagosome formation, but the amount of phospholipid that is imported by these vesicles is thought to be much smaller than that transported by the Atg2-dependent nonvesicular mechanism (Chowdhury et al., 2018; Kotani et al., 2018; Maeda et al., 2019; Osawa et al., 2019; Valverde et al., 2019; Yamamoto et al., 2012). Thus, the symmetrical distribution of PtdCho and PtdSer is more likely to be caused by the transbilayer movement of phospholipids in isolation membranes/autophagosomes.

Symmetrical distribution of PtdIns(4)P in autophagic membranes

PtdIns(4)P is known to play important roles in autophagy (Palamiuc et al., 2020). To label PtdIns(4)P in QF-FRL, we adopted the PtdIns(4)P-binding domain of SidM/DrrA (P4M) of *Legionella pneumophila*, which has a high affinity for this lipid (Brombacher et al., 2009; Schoebel et al., 2010) and has been used successfully as a fluorescence biosensor in live cells (Hammond et al., 2014). We first confirmed that GST-tagged P4M (GST-P4M) specifically labels PtdIns(4)P in liposome freeze-fracture replicas (Fig. S2 A). With this probe, intense labeling for PtdIns(4)P was found in the cytoplasmic leaflet of the Golgi, the vacuole, and the plasma membrane in yeast in growth condition (Fig. S2, B and D). GST-P4M^{K568A}, a P4M mutant that lacks the PtdIns(4)P binding affinity due to one amino acid substitution (Del Campo et al., 2014), did not bind to any membrane significantly, verifying the specificity of this labeling method (Fig. S2, C and D).

In yeast cultured in S(–NC) for 4 h, PtdIns(4)P was labeled in autophagosomes and autophagic bodies in both the cytoplasmic and the noncytoplasmic leaflets (Fig. 3, A and B). Vacuoles in autophagic cells showed a significant increase in PtdIns(4)P labeling in the lumenal leaflet compared with the amount observed in growth condition (Fig. 3 C), as observed for PtdSer. The result in autophagosomes is similar to that in a recent report

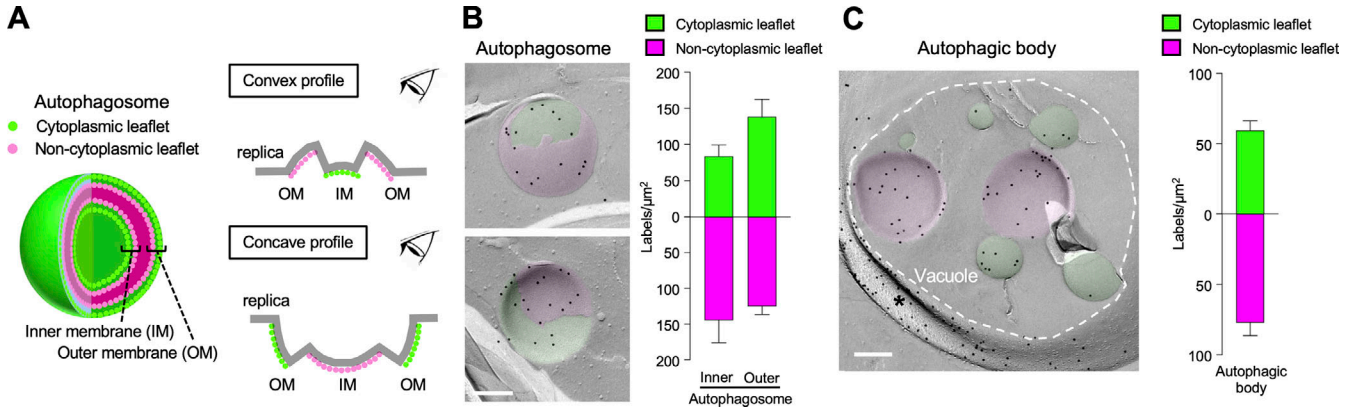

Figure 1. **Distribution of PtdCho labeled metabolically with propargylcholine. Yeast cultured in S(–NC) for 4 h. (A)** The illustration shows the two patterns of autophagosome freeze fracturing. The outer membranes (OMs) and inner membranes (IMs) can be distinguished by their convexity/concavity and by whether the membrane is observed nearer or farther. **(B)** Autophagosomes. The cytoplasmic and noncytoplasmic leaflets are colored green and pink, respectively, in this and subsequent figures. Scale bar, 0.2 µm. The bar graph shows the density of PtdCho labels in the cytoplasmic and noncytoplasmic leaflets. *n* = 16; pooled data from three independent experiments; mean ± SEM. **(C)** Autophagic bodies. Scale bar, 0.2 µm. The graph shows the PtdCho label density. *n* = 39 (cytoplasmic), 35 (noncytoplasmic); pooled data from three independent experiments; mean ± SEM; *, the noncytoplasmic leaflet of the vacuole.

that used an anti-PtdIns(4)P antibody as a probe, but the PtdIns(4)P antibody method yielded only a low level of labeling in the autophagic bodies and in the cytoplasmic leaflet of vacuoles (Kurokawa et al., 2019; Tomioku et al., 2018). The reason for these discrepancies is not clear, but the PtdIns(4)P distribution detected by GST-P4M is consistent with the fact that autophagic bodies originate from inner autophagosomal membranes and with the presence of PtdIns 4-kinase Lsb6 on the vacuolar membrane (Han et al., 2002).

The symmetrical distribution of PtdIns(4)P in autophagosomes and autophagic bodies is conspicuous, because this lipid is generated by kinases and phosphatases in the cytosol (Strahl and Thorner, 2007), and no other membrane shows significant labeling in the noncytoplasmic leaflet (Fig. S2 D). This distribution is similar to that of PtdIns(3)P, which is localized in the noncytoplasmic leaflet of autophagic membranes, despite its synthesis in the cytoplasmic leaflet (Cheng et al., 2014). If only one lipid were to show such distribution, it might appear that some special mechanism was operating only on that lipid. The presence of both PtdIns(3)P and PtdIns(4)P in the noncytoplasmic leaflet, however, suggests a general mechanism that enables transbilayer phospholipid movement in isolation membranes/autophagosomes.

De novo–synthesized PtdCho quickly attains symmetrical distribution

To further test the idea of phospholipid translocation in isolation membranes/autophagosomes, we examined whether PtdCho attains symmetrical distribution immediately after synthesis. For this purpose, PtdCho was labeled metabolically for only 30 min. First, to examine how de novo–synthesized PtdCho is incorporated into yeast in growth condition, propargylcholine was added to the SC medium only for the last 30 min before

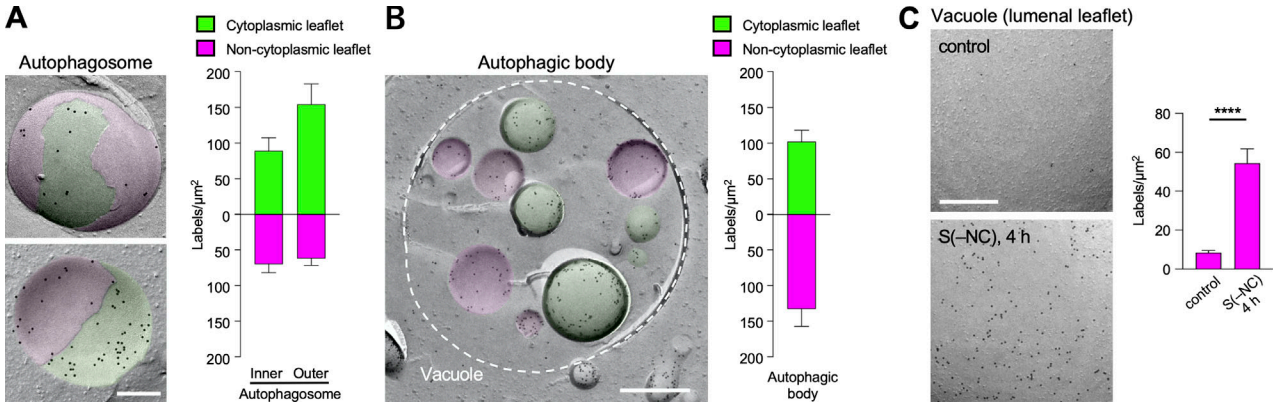

Figure 2. **PtdSer labeling in yeast cultured in S(–NC) for 4 h. (A)** Autophagosomes. Scale bar, 0.2 µm. The graph shows the PtdSer label density. *n* = 37 (inner cytoplasmic, outer noncytoplasmic), 32 (outer cytoplasmic, inner noncytoplasmic); pooled data from three independent experiments; mean ± SEM. **(B)** Autophagic bodies. Scale bar, 0.5 µm. The graph shows the PtdSer label density. *n* = 31; pooled data from three independent experiments; mean ± SEM. **(C)** The lumenal leaflet of vacuoles. Scale bar, 0.2 µm. The graph shows the PtdSer labeling density in growth phase (control) and after autophagy induction in S(–NC) for 4 h. *n* = 32; pooled data from three independent experiments; mean ± SEM. ****, P < 0.0001, Mann–Whitney test.

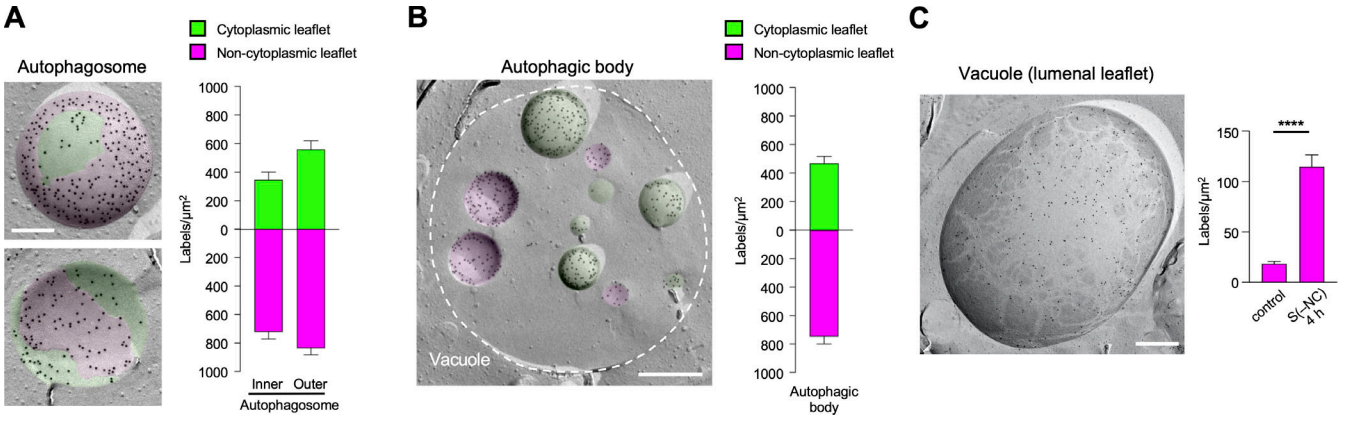

Figure 3. **PtdIns(4)P labeling in yeast cultured in S(–NC) for 4 h. (A)** Autophagosomes. Scale bar, 0.2 µm. The graph shows the PtdIns(4)P label density. *n* = 32 (inner cytoplasmic, outer noncytoplasmic), 30 (outer cytoplasmic, inner noncytoplasmic); pooled data from four independent experiments; mean ± SEM. **(B)** Autophagic bodies. Scale bar, 0.5 µm. The graph shows the PtdIns(4)P label density. *n* = 33 (cytoplasmic), 35 (noncytoplasmic); pooled data from four independent experiments; mean ± SEM. **(C)** Lumenal leaflet of vacuoles. Scale bar, 0.5 µm. The graph shows the PtdIns(4)P labeling density in growth phase (control) and after autophagy induction. *n* = 30; pooled data from four independent experiments; mean ± SEM. ****, P < 0.0001, Mann–Whitney test.

freezing. The PtdCho label was distributed most densely in the outer nuclear membrane, the cortical ER, and the outer mitochondrial membrane, and much less densely in the inner mitochondrial membrane, the vacuole, and the plasma membrane (Figs. 4 A and S3 A). This result was consistent with the putative distribution of Cpt1 and Ept1, enzymes of the Kennedy pathway synthesizing PtdCho, in the ER and mitochondria (Henry et al., 2012).

Distribution of de novo–synthesized PtdCho in autophagy was similarly examined. After autophagy was induced for 3.5 h in S(–NC), propargylcholine was added; 30 min later, yeast was frozen. By this means, autophagosomal membranes were significantly labeled, whereas autophagic bodies and other organelles, including the nuclear membrane, the cortical ER, and the outer mitochondrial membrane, were labeled only scarcely (Figs. 4 B and S3 B). The difference between autophagosomes and other organelles was evident even when the labeling density was compared within the same cell, refuting the possibility of cell-to-cell variation (Fig. 4 C). The contrasting distribution of de novo–synthesized PtdCho in growth condition and after autophagy induction was confirmed by fluorescence microscopy. In yeast in SC medium, intense click labeling was seen in the ER and mitochondria; after incubation in S(–NC), in contrast, the labeling was observed only as a weak dot overlapping with GFP-Atg8 (Fig. S3 C).

Remarkably, de novo–synthesized PtdCho was distributed in both leaflets of autophagosomes at comparable densities (Fig. 4 D). Phospholipid scrambling is thought to occur constitutively in the ER (Pomorski and Menon, 2016), but the negligible labeling in the ER makes it unlikely that the symmetrical PtdCho distribution in autophagosomes is generated by the putative ER mechanism. Rather, our result more likely indicates phospholipid translocation in isolation membranes/autophagosomes, which is probably mediated by Atg9 (Matoba et al., 2020). Consistently, in *atg9Δ* cells that are reconstituted with an Atg9 mutant, Atg9^{Basic}, incorporation of de novo–synthesized PtdCho into the noncytoplasmic leaflet of the autophagosomal membranes was decreased (Fig. 4 E). The decrease was relatively small, but this is reasonable considering that the difference of the in vitro phospholipid translocation activity between WT Atg9 and Atg9^{Basic} is ∼18% (Matoba et al., 2020).

The above result also indicates that PtdCho synthesized by the Kennedy pathway during autophagy is preferentially incorporated into isolation membranes. This is in line with the recent report showing that phospholipid synthesis for isolation membrane expansion is driven by Faa1 that exists in the vicinity (Schütter et al., 2020). Phosphatidylinositol synthase was also shown to be enriched in an ER subdomain near the autophagosome formation site (Nishimura et al., 2017). These results corroborate the idea that a dedicated molecular machinery for phospholipid synthesis and transport is involved in isolation membrane formation.

Based on the available data, including those on the molecular functions of Atg2 and Atg9 in vitro (Kotani et al., 2018; Matoba et al., 2020; Osawa et al., 2019), we propose that autophagy in yeast involves the following sequence of events: Phospholipids are synthesized in an ER domain near the ERES, transported to nascent isolation membranes via Atg2 at the membrane contact site, and distributed into both leaflets of the membrane by Atg9, thereby inducing proportionate membrane growth (Fig. 4 F). Considering that mammalian ATG2A and ATG9A share functionality with their respective yeast counterparts (Chowdhury et al., 2018; Maeda et al., 2019; Maeda et al., 2020; Matoba et al., 2020; Valverde et al., 2019), autophagy in mammalian cells is likely to involve similar processes. In this respect, it is peculiar that PtdIns(3)P in autophagosomal membranes is significantly labeled only in the cytoplasmic leaflet in mammalian cells, whereas it is labeled in both leaflets in yeast (Cheng et al., 2014). We speculate that this apparent difference may have several causes, which are discussed below. Phospholipid scrambling by Atg9 (ATG9A) is likely to occur near Atg2 (ATG2A) at the ER isolation membrane contact site (Gómez-Sanchez et al., 2018; Tang et al., 2019; Guardia et al., 2020), suggesting that phospholipids that are transported from the ER are preferentially

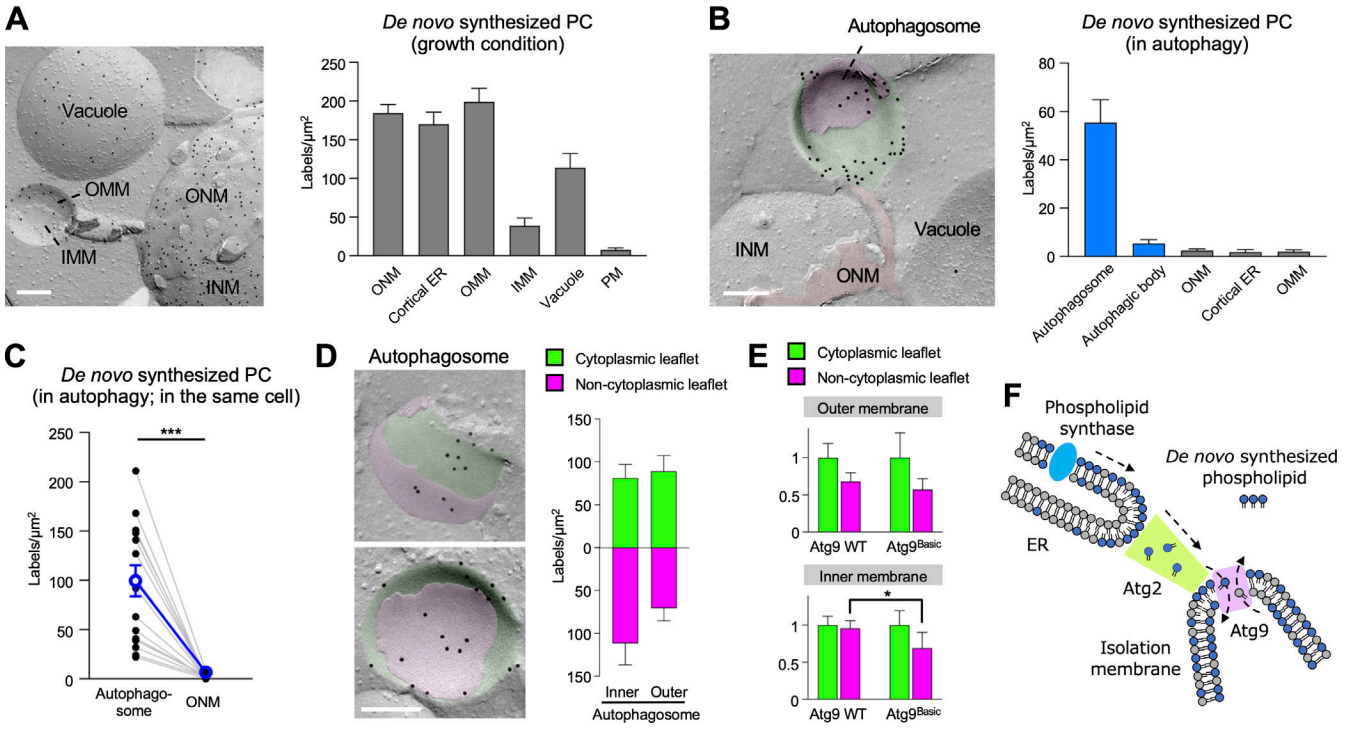

Figure 4. **Labeling of de novo–synthesized PtdCho.** Propargylcholine was added to medium 30 min before freezing. **(A)** Normal growth condition in SC medium. The outer nuclear membranes (ONMs), the cortical ER, the outer mitochondrial membrane (OMM) and inner mitochondrial membrane (IMM), the vacuole, and the plasma membrane (PM) are shown. See additional micrographs in Fig. S3 A. Scale bar, 0.2 µm. The density of PtdCho label. *n* = 15 (ONM), 16 (cortical ER), 17 (OMM), 15 (IMM), 18 (vacuole), 15 (PM); pooled data from three independent experiments; mean ± SEM. **(B)** After autophagic induction in S(−NC). See additional micrographs in Fig. S3 B. Scale bar, 0.2 µm. The density of PtdCho label. *n* = 54 (autophagosome), 38 (autophagic body), 21 (ONM), 15 (cortical ER), 19 (OMM); pooled data from three independent experiments; mean ± SEM. Please note that the labeling densities in the ONM, the cortical ER, and the OMM are much lower here than they are in growth condition (Fig. 4 A). **(C)** Comparison of the labeling density in autophagosomes and the ONM in the same cell. Gray lines connect the labeling densities in a cell. *n* = 15; pooled data from three independent experiments; mean ± SEM is shown by blue circles and error bars. ***, P < 0.001, two-tailed Wilcoxon signed rank test. **(D)** The label intensity in the respective leaflets of autophagosomal membranes. Scale bar, 0.2 µm. *n* = 19 (inner cytoplasmic, outer noncytoplasmic), 22 (outer cytoplasmic, inner noncytoplasmic); pooled data from three independent experiments; mean ± SEM. **(E)** Comparison of *atg9Δ* cells expressing WT Atg9 or Atg9^{Basic}. PtdCho labels in autophagosomal membranes. The label intensities in the noncytoplasmic leaflet are normalized to the average label intensities in the cytoplasmic leaflet. *n* = 18 (inner cytoplasmic, outer noncytoplasmic), 22 (outer cytoplasmic, inner noncytoplasmic; Atg9 WT); 20 (inner cytoplasmic, outer noncytoplasmic), 16 (outer cytoplasmic, inner noncytoplasmic; Atg9^{Basic}); pooled data from three independent experiments; mean ± SEM. *, P < 0.05, Mann–Whitney test. **(F)** Diagram showing the putative phospholipid transport mechanism during isolation membrane expansion (see text for details).

translocated to the noncytoplasmic leaflet. Here, mammalian autophagosomes are larger than yeast autophagosomes, and they require more phospholipid influx. In this setting, PtdIns(3)P, which is present in a relatively sparse manner in mammalian autophagosomes (Cheng et al., 2014), may not undergo efficient scrambling by ATG9A. Additionally, the distribution density of mammalian ATG9A in autophagosomal membranes is likely to be smaller than that of yeast Atg9 (Koyama-Honda et al., 2013; Orsi et al., 2012; Yamamoto et al., 2012), and PtdIns(3)P-binding proteins that are likely to restrict PtdIns(3)P scrambling might exist more abundantly in mammalian cells than in yeast (Dall'Armi et al., 2013; Lystad and Simonsen, 2016). A combination of these and other quantitative differences probably gives rise to the distinct PtdIns(3)P distribution patterns in yeast and mammalian autophagosomal membranes.

Despite the emergence of a plausible model for the isolation membrane formation, the in vivo functionalities of Atg2 and Atg9 are yet to be defined in detail, as are the means by which they are regulated. Moreover, it is not clear how phospholipids synthesized in a limited ER domain can be funneled to isolation membrane formation rather than diffusing into the general ER membrane. These questions need to be addressed in further studies before we can fully understand the mechanisms of isolation membrane formation.

Materials and methods

Probes

For PtdIns(4)P labeling, the P4M domain of SidM/DrrA (Brombacher et al., 2009) was cloned from *L. pneumophila* cDNA (provided by Dr. Koji Kimura, Nagoya University Graduate School of Medicine, Nagoya, Japan) and inserted to a pGEX-6P vector (GE Healthcare). Recombinant GST-P4M and its mutant GST- P4M^{K568A} were produced in *E. coli* of the BL21 (DE3) strain and affinity purified by using glutathione-agarose (Sigma-Aldrich). For PtdSer labeling, vectors carrying the PH domain of human evectin-2 in tandem (Uchida et al., 2011) were kindly provided by Dr. Tomohiko Taguchi (Tohoku University, Sendai, Japan), and the recombinant

GST-evectin-2-2xPH domain was produced after subcloning to pGEX-6P (Tsuji et al., 2019). Rabbit anti-GST (A190-122A; Bethyl) and mouse anti-biotin (200–002-211; Jackson ImmunoResearch) antibodies were obtained from their respective suppliers. Colloidal gold (10 nm)–conjugated Protein A (PAG10; The University Medical Center Utrecht) and goat anti-mouse IgG antibody (GAM12; Jackson ImmunoResearch) were also purchased.

Liposomes

1-Palmitoyl-2-oleoyl-sn-glycero-3-phosphocholine (MC-6081; Nichiyu), L-α-phosphatidylinositol (bovine liver; 840042P; Avanti), PtdIns(3)P (910; CellSignals), PtdIns(4)P (912; CellSignals), phosphatidylinositol 5-phosphate (914; CellSignals), phosphatidylinositol 3,4-bisphosphate (904; CellSignals), phosphatidylinositol 3,5-bisphosphate (906; CellSignals), phosphatidylinositol 4,5-bisphosphate (902; CellSignals), and phosphatidylinositol 3,4,5-trisphosphate (908; CellSignals) were dissolved in chloroform/methanol (2:1) at defined molar ratios, dried with dry nitrogen gas in a hot bath, and desiccated in a vacuum overnight. Dried samples were vortexed with 20 mM Hepes buffer containing 0.1% rhodamine-dioleoyl phosphatidylethanolamine (810150; Avanti) at 37°C, and the solution was pushed through a mini-extruder (Avanti) with a polycarbonate membrane filter (pore size, 0.2 µm) 10 times to create unilamellar vesicles. These were centrifuged for 30 min at 50,000 *g* in a Beckman Optima TLX ultracentrifuge, and the pellet was quick frozen.

Yeast

The *S. cerevisiae* strains used in this study are derived from SEY6210 and W303-1A and are listed in Table S1. Deletion mutants were generated according to a PCR-based method using pFA6a plasmids as templates (Kaiser et al., 1994). For comparison of WT Atg9 and Atg9^{Basic}, *atg9Δ* cells expressing pRS316-ScAtg9^{WT}-EGFP (pRS316-ScAtg9^{WT}) and pRS316-ScAtg9^{Basic}-EGFP (p9KM129) were used (Matoba et al., 2020).

Yeast cells were grown to the exponential phase in SC medium (0.17% yeast nitrogen base without amino acids and ammonium sulfate [233520; Becton Dickinson], 0.5% ammonium sulfate, 2% glucose, and dropout mix) at 30°C. For metabolic labeling of PtdCho, the medium was supplemented with 1 mM propargylcholine, which was synthesized as described (Jao et al., 2009). To induce autophagy, cells were washed with distilled water and incubated for 4 h at 30°C in S(–NC). Vacuolar proteolysis was blocked by adding 1 mM phenylmethylsulphonyl fluoride (10837091001; Sigma-Aldrich) or by using *pep4Δ* cells to observe autophagic bodies.

Quick freezing and freeze fracture

A copper EM grid (100 mesh) immersed with yeast or liposome pellets was sandwiched between a 20-µm-thick copper foil and a flat aluminum disc (242; Engineering Office M. Wohlwend) and frozen using an HPM 010 high-pressure freezing machine (Leica). For freeze fracture, the sandwiched sample was transferred to the stage of a Balzers BAF 400 and fractured at −115°C to −105°C under a vacuum of ∼10^{-6} mbar. Replicas were made by electron-beam evaporation in three steps: carbon (C; 5 nm in thickness) at an angle of 90° to the fractured surface, platinum-C (2 nm) at an angle of 45°, and C (10 nm) at an angle of 90°. The thickness of evaporation was adjusted by referring to a quartz crystal thickness monitor.

Replicas were treated sequentially with 2.5% SDS in 0.1 M Tris-HCl (pH 8.0) overnight at 60°C, with 0.1 mg/ml Zymolyase 100T (07665–55; Nacalai) in PBS containing 0.1% Triton X-100, 1% BSA (01281–26; Nacalai), and a protease inhibitor cocktail (25955–11; Nacalai) for 2 h at 37°C, and again with 2.5% SDS in PBS overnight at 60°C. In some experiments, the Zymolyase step was replaced with digestion with 0.5% Westase (9005; Takara Bio) in McIlvain citrate phosphate buffer (pH 6.0) containing 10 mM EDTA and 30% FCS (Tsuji et al., 2019). The replicas were stored in buffered 50% glycerol in PBS at −20°C until use.

PtdCho labeling

PtdCho in all cellular membranes was labeled metabolically by culturing yeast overnight in growth medium supplemented with 1 mM propargylcholine. For labeling de novo–synthesized PtdCho, yeast cultured in medium without propargylcholine was treated with 1 mM propargylcholine only for 30 min before quick freezing. Click labeling of PtdCho was performed as described (Iyoshi et al., 2014) with a slight modification. For EM, freeze-fracture replicas were treated with 2% cold fish gelatin (G7041; Sigma-Aldrich) and 0.001% Triton X-100 in 0.1 M Tris-HCl (pH 7.5) for 10 min and incubated in 0.1 M Tris-HCl (pH 7.5) containing 1 mM copper sulfate, 2.5 mM ascorbic acid, 100 µM Tris[(1-benzyl-1*H*-1,2,3-triazol-4-yl)methyl]amine (AS-63360; AnaSpec), 2% cold fish gelatin, and 5 µM biotin-azide (BCFA-003-1; baseclick) for 30 min at RT. After rinsing, the replicas were blocked with 2% cold fish gelatin in PBS for 30 min and incubated with mouse anti-biotin antibody (8.7 µg/ml) in PBS containing 1% cold fish gelatin overnight at 4°C, followed by GAM12 for 30 min at 37°C in PBS containing 1% BSA. For fluorescence microscopy, yeast cells were fixed in 4% formaldehyde in 0.1 M sodium phosphate buffer for 15 min, permeabilized with 0.1% Triton X-100 in PBS for 10 min, and subjected to the click reaction for 20 min at RT. The reaction solution contained 0.1 mM copper sulfate, 0.1 M ascorbic acid, and 500 nM AFDye546 picolyl-azide (1283-1; Click Chemistry Tools) in 0.1 M Tris-HCl (pH 7.5). After rinsing, cells were observed under an Axiovert 200 M microscope (Zeiss) equipped with Apotome2 using an Apochromat 63× objective lens. The color, brightness, and contrast of the presented images were adjusted using Adobe Photoshop CC.

PtdSer labeling

PtdSer was labeled as described (Tsuji et al., 2019). Briefly, freeze-fracture replicas were blocked with a mixture of 3% BSA and 2% cold fish gelatin in 0.1 M sodium phosphate buffer (pH 6.0) and incubated at 4°C overnight with GST-evectin-2 2xPH in 0.1 M sodium phosphate buffer containing 1% BSA and 1% cold fish gelatin. Samples were then successively incubated in PBS containing 1% BSA at 37°C for 40 min with a rabbit anti-GST antibody, then for another 40 min with colloidal gold (10 nm)–conjugated protein A.

PtdIns(4)P labeling

For PtdIns(4)P labeling, replicas were washed with PBS containing 0.1% Triton X-100, blocked with 3% BSA and 2% cold fish

gelatin in PBS, and incubated overnight at 4°C with GST-P4M or GST-P4M^{K568A} (80 ng/ml) in PBS containing 1% BSA and 1% cold fish gelatin. Samples were subsequently treated with rabbit anti-GST antibody (10 µg/ml) followed by colloidal gold (10 nm)–conjugated protein A (1:50 dilution of the supplied solution), both for 30 min at 37°C in 1% BSA in PBS.

EM observation and data analysis

The labeled replicas were picked up on Formvar-coated EM grids after a brief rinse in distilled water and observed under a JEOL JEM-1011 electron microscope. Digital images were taken using a charge-coupled device camera (Gatan). The number of colloidal gold particles was counted manually, and areas were measured using ImageJ (National Institutes of Health). The labeling density in the selected structure was calculated by dividing the number of colloidal gold particles by the area. For each structure, more than 15 different micrographs that were taken randomly were used. Each experiment was repeated more than three times to confirm reproducibility. Statistical differences between samples were tested by two-tailed Mann–Whitney *U* test using Prism 8 (GraphPad Software). The labeling intensity in the autophagosome of each cell was compared with that in the outer nuclear membrane of the same cell by the Wilcoxon signed-rank test using the statistical language R (Fig. 4 C).

Online supplemental material

Fig. S1 shows the outline of freeze-fracture replica labeling. Fig. S2 shows the labeling of PtdIns(4)P. Fig. S3 shows the labeling of de novo–synthesized PtdCho. Table S1 lists the yeast strains used in this study.

Acknowledgments

We thank Dr. Koji Kimura (Nagoya University) for *L. pneumophila* cDNA; Dr. Tomohiko Taguchi (Tohoku University) for plasmids carrying the evectin-2 PH domain in tandem; Drs. Hitoshi Nakatogawa and Tetsuya Kotani (Tokyo Institute of Technology, Tokyo, Japan) for W303-1A strains; Ms. Tsuyako Tatematsu, Dr. Jinglei Cheng (Nagoya University), and Ms. Hiroko Osakada (Juntendo University) for excellent technical assistance; and Drs. Hitoshi Nakatogawa and Nobuo N. Noda (Institute of Microbial Chemistry) for critical reading of the manuscript.

This study was supported by Grants-in-Aid for Scientific Research from the Japan Society of the Promotion of Science (18K15004 to M. Orii, 19K07265 and 20H05339 to T. Tsuji, and 15H05902 and 18H04023 to T. Fujimoto).

The authors declare no competing financial interests.

Author contributions: Conceptualization: T. Fujimoto; investigation: M. Orii, T. Tsuji, and Y. Ogasawara; writing, original draft: M. Orii and T. Fujimoto; writing, review and editing: T. Fujimoto; funding acquisition: M. Orii, T. Tsuji, and T. Fujimoto.

Submitted: 28 September 2020
Revised: 14 December 2020
Accepted: 17 December 2020

References

Bento, C.F., M. Renna, G. Ghislat, C. Puri, A. Ashkenazi, M. Vicinanza, F.M. Menzies, and D.C. Rubinsztein. 2016. Mammalian autophagy: How does it work? *Annu. Rev. Biochem.* 85:685–713. https://doi.org/10.1146/annurev-biochem-060815-014556

Brombacher, E., S. Urwyler, C. Ragaz, S.S. Weber, K. Kami, M. Overduin, and H. Hilbi. 2009. Rab1 guanine nucleotide exchange factor SidM is a major phosphatidylinositol 4-phosphate-binding effector protein of Legionella pneumophila. *J. Biol. Chem.* 284:4846–4856. https://doi.org/10.1074/jbc.M807505200

Cheng, J., A. Fujita, H. Yamamoto, T. Tatematsu, S. Kakuta, K. Obara, Y. Ohsumi, and T. Fujimoto. 2014. Yeast and mammalian autophagosomes exhibit distinct phosphatidylinositol 3-phosphate asymmetries. *Nat. Commun.* 5:3207. https://doi.org/10.1038/ncomms4207

Chowdhury, S., C. Otomo, A. Leitner, K. Ohashi, R. Aebersold, G.C. Lander, and T. Otomo. 2018. Insights into autophagosome biogenesis from structural and biochemical analyses of the ATG2A-WIPI4 complex. *Proc. Natl. Acad. Sci. USA.* 115:E9792–E9801. https://doi.org/10.1073/pnas.1811874115

Dall'Armi, C., K.A. Devereaux, and G. Di Paolo. 2013. The role of lipids in the control of autophagy. *Curr. Biol.* 23:R33–R45. https://doi.org/10.1016/j.cub.2012.10.041

Del Campo, C.M., A.K. Mishra, Y.H. Wang, C.R. Roy, P.A. Janmey, and D.G. Lambright. 2014. Structural basis for PI(4)P-specific membrane recruitment of the Legionella pneumophila effector DrrA/SidM. *Structure.* 22:397–408. https://doi.org/10.1016/j.str.2013.12.018

Gómez-Sánchez, R., J. Rose, R. Guimarães, M. Mari, D. Papinski, E. Rieter, W.J. Geerts, R. Hardenberg, C. Kraft, C. Ungermann, and F. Reggiori. 2018. Atg9 establishes Atg2-dependent contact sites between the endoplasmic reticulum and phagophores. *J. Cell Biol.* 217:2743–2763. https://doi.org/10.1083/jcb.201710116

Graef, M., J.R. Friedman, C. Graham, M. Babu, and J. Nunnari. 2013. ER exit sites are physical and functional core autophagosome biogenesis components. *Mol. Biol. Cell.* 24:2918–2931. https://doi.org/10.1091/mbc.e13-07-0381

Guardia, C.M., X.F. Tan, T. Lian, M.S. Rana, W. Zhou, E.T. Christenson, A.J. Lowry, J.D. Faraldo-Gómez, J.S. Bonifacino, J. Jiang, and A. Banerjee. 2020. Structure of human ATG9A, the only transmembrane protein of the core autophagy machinery. *Cell Rep.* 31:107837. https://doi.org/10.1016/j.celrep.2020.107837

Hammond, G.R., M.P. Machner, and T. Balla. 2014. A novel probe for phosphatidylinositol 4-phosphate reveals multiple pools beyond the Golgi. *J. Cell Biol.* 205:113–126. https://doi.org/10.1083/jcb.201312072

Han, G.S., A. Audhya, D.J. Markley, S.D. Emr, and G.M. Carman. 2002. The Saccharomyces cerevisiae LSB6 gene encodes phosphatidylinositol 4-kinase activity. *J. Biol. Chem.* 277:47709–47718. https://doi.org/10.1074/jbc.M207996200

Henry, S.A., S.D. Kohlwein, and G.M. Carman. 2012. Metabolism and regulation of glycerolipids in the yeast Saccharomyces cerevisiae. *Genetics.* 190:317–349. https://doi.org/10.1534/genetics.111.130286

Iyoshi, S., J. Cheng, T. Tatematsu, S. Takatori, M. Taki, Y. Yamamoto, A. Salic, and T. Fujimoto. 2014. Asymmetrical distribution of choline phospholipids revealed by click chemistry and freeze-fracture electron microscopy. *ACS Chem. Biol.* 9:2217–2222. https://doi.org/10.1021/cb500558n

Jao, C.Y., M. Roth, R. Welti, and A. Salic. 2009. Metabolic labeling and direct imaging of choline phospholipids in vivo. *Proc. Natl. Acad. Sci. USA.* 106:15332–15337. https://doi.org/10.1073/pnas.0907864106

Kaiser, C., S. Michaelis, and A. Mitchell. 1994. Methods in Yeast Genetics. Cold Spring Harbor Laboratory, Cold Spring Harbor, NY.

Kishi-Itakura, C., I. Koyama-Honda, E. Itakura, and N. Mizushima. 2014. Ultrastructural analysis of autophagosome organization using mammalian autophagy-deficient cells. *J. Cell Sci.* 127:4089–4102. https://doi.org/10.1242/jcs.156034

Kotani, T., H. Kirisako, M. Koizumi, Y. Ohsumi, and H. Nakatogawa. 2018. The Atg2-Atg18 complex tethers pre-autophagosomal membranes to the endoplasmic reticulum for autophagosome formation. *Proc. Natl. Acad. Sci. USA.* 115:10363–10368. https://doi.org/10.1073/pnas.1806727115

Koyama-Honda, I., E. Itakura, T.K. Fujiwara, and N. Mizushima. 2013. Temporal analysis of recruitment of mammalian ATG proteins to the autophagosome formation site. *Autophagy.* 9:1491–1499. https://doi.org/10.4161/auto.25529

Kurokawa, Y., R. Konishi, A. Yoshida, K. Tomioku, T. Futagami, H. Tamaki, K. Tanabe, and A. Fujita. 2019. Essential and distinct roles of phosphatidylinositol

4-kinases, Pik1p and Stt4p, in yeast autophagy. *Biochim. Biophys. Acta Mol. Cell Biol. Lipids*. 1864:1214–1225. https://doi.org/10.1016/j.bbalip.2019.05.004

Lystad, A.H., and A. Simonsen. 2016. Phosphoinositide-binding proteins in autophagy. *FEBS Lett.* 590:2454–2468. https://doi.org/10.1002/1873-3468.12286

Maeda, S., C. Otomo, and T. Otomo. 2019. The autophagic membrane tether ATG2A transfers lipids between membranes. *eLife.* 8:e45777. https://doi.org/10.7554/eLife.45777

Maeda, S., H. Yamamoto, L.N. Kinch, C.M. Garza, S. Takahashi, C. Otomo, N.V. Grishin, S. Forli, N. Mizushima, and T. Otomo. 2020. Structure, lipid scrambling activity and role in autophagosome formation of ATG9A. *Nat. Struct. Mol. Biol.* 27:1194–1201. https://doi.org/10.1038/s41594-020-00520-2

Matoba, K., T. Kotani, A. Tsutsumi, T. Tsuji, T. Mori, D. Noshiro, Y. Sugita, N. Nomura, S. Iwata, Y. Ohsumi, et al. 2020. Atg9 is a lipid scramblase that mediates autophagosomal membrane expansion. *Nat. Struct. Mol. Biol.* 27:1185–1193. https://doi.org/10.1038/s41594-020-00518-w

Mizushima, N., T. Yoshimori, and Y. Ohsumi. 2011. The role of Atg proteins in autophagosome formation. *Annu. Rev. Cell Dev. Biol.* 27:107–132. https://doi.org/10.1146/annurev-cellbio-092910-154005

Nakatogawa, H. 2020. Mechanisms governing autophagosome biogenesis. *Nat. Rev. Mol. Cell Biol.* 21:439–458. https://doi.org/10.1038/s41580-020-0241-0

Nishimura, T., N. Tamura, N. Kono, Y. Shimanaka, H. Arai, H. Yamamoto, and N. Mizushima. 2017. Autophagosome formation is initiated at phosphatidylinositol synthase-enriched ER subdomains. *EMBO J.* 36:1719–1735. https://doi.org/10.15252/embj.201695189

Orsi, A., M. Razi, H.C. Dooley, D. Robinson, A.E. Weston, L.M. Collinson, and S.A. Tooze. 2012. Dynamic and transient interactions of Atg9 with autophagosomes, but not membrane integration, are required for autophagy. *Mol. Biol. Cell.* 23:1860–1873. https://doi.org/10.1091/mbc.e11-09-0746

Osawa, T., T. Kotani, T. Kawaoka, E. Hirata, K. Suzuki, H. Nakatogawa, Y. Ohsumi, and N.N. Noda. 2019. Atg2 mediates direct lipid transfer between membranes for autophagosome formation. *Nat. Struct. Mol. Biol.* 26:281–288. https://doi.org/10.1038/s41594-019-0203-4

Palamiuc, L., A. Ravi, and B.M. Emerling. 2020. Phosphoinositides in autophagy: current roles and future insights. *FEBS J.* 287:222–238. https://doi.org/10.1111/febs.15127

Pomorski, T.G., and A.K. Menon. 2016. Lipid somersaults: Uncovering the mechanisms of protein-mediated lipid flipping. *Prog. Lipid Res.* 64:69–84. https://doi.org/10.1016/j.plipres.2016.08.003

Sawa-Makarska, J., V. Baumann, N. Coudevylle, S. von Bülow, V. Nogellova, C. Abert, M. Schuschnig, M. Graef, G. Hummer, and S. Martens. 2020. Reconstitution of autophagosome nucleation defines Atg9 vesicles as seeds for membrane formation. *Science.* 369:eaaz7714. https://doi.org/10.1126/science.aaz7714

Schoebel, S., W. Blankenfeldt, R.S. Goody, and A. Itzen. 2010. High-affinity binding of phosphatidylinositol 4-phosphate by Legionella pneumophila DrrA. *EMBO Rep.* 11:598–604. https://doi.org/10.1038/embor.2010.97

Schütter, M., P. Giavalisco, S. Brodesser, and M. Graef. 2020. Local fatty acid channeling into phospholipid synthesis drives phagophore expansion during autophagy. *Cell.* 180:135–149.e14. https://doi.org/10.1016/j.cell.2019.12.005

Strahl, T., and J. Thorner. 2007. Synthesis and function of membrane phosphoinositides in budding yeast, Saccharomyces cerevisiae. *Biochim. Biophys. Acta.* 1771:353–404. https://doi.org/10.1016/j.bbalip.2007.01.015

Suzuki, K., M. Akioka, C. Kondo-Kakuta, H. Yamamoto, and Y. Ohsumi. 2013. Fine mapping of autophagy-related proteins during autophagosome formation in Saccharomyces cerevisiae. *J. Cell Sci.* 126:2534–2544. https://doi.org/10.1242/jcs.122960

Tang, Z., Y. Takahashi, H. He, T. Hattori, C. Chen, X. Liang, H. Chen, M.M. Young, and H.G. Wang. 2019. TOM40 Targets Atg2 to Mitochondria-Associated ER Membranes for Phagophore Expansion. *Cell Rep.* 28:1744–1757.e5.

Tomioku, K.N., M. Shigekuni, H. Hayashi, A. Yoshida, T. Futagami, H. Tamaki, K. Tanabe, and A. Fujita. 2018. Nanoscale domain formation of phosphatidylinositol 4-phosphate in the plasma and vacuolar membranes of living yeast cells. *Eur. J. Cell Biol.* 97:269–278. https://doi.org/10.1016/j.ejcb.2018.03.007

Tsuji, T., J. Cheng, T. Tatematsu, A. Ebata, H. Kamikawa, A. Fujita, S. Gyobu, K. Segawa, H. Arai, T. Taguchi, et al. 2019. Predominant localization of phosphatidylserine at the cytoplasmic leaflet of the ER, and its TMEM16K-dependent redistribution. *Proc. Natl. Acad. Sci. USA.* 116:13368–13373. https://doi.org/10.1073/pnas.1822025116

Uchida, Y., J. Hasegawa, D. Chinnapen, T. Inoue, S. Okazaki, R. Kato, S. Wakatsuki, R. Misaki, M. Koike, Y. Uchiyama, et al. 2011. Intracellular phosphatidylserine is essential for retrograde membrane traffic through endosomes. *Proc. Natl. Acad. Sci. USA.* 108:15846–15851. https://doi.org/10.1073/pnas.1109101108

Valverde, D.P., S. Yu, V. Boggavarapu, N. Kumar, J.A. Lees, T. Walz, K.M. Reinisch, and T.J. Melia. 2019. ATG2 transports lipids to promote autophagosome biogenesis. *J. Cell Biol.* 218:1787–1798. https://doi.org/10.1083/jcb.201811139

Velikkakath, A.K., T. Nishimura, E. Oita, N. Ishihara, and N. Mizushima. 2012. Mammalian Atg2 proteins are essential for autophagosome formation and important for regulation of size and distribution of lipid droplets. *Mol. Biol. Cell.* 23:896–909. https://doi.org/10.1091/mbc.e11-09-0785

Yamamoto, H., S. Kakuta, T.M. Watanabe, A. Kitamura, T. Sekito, C. Kondo-Kakuta, R. Ichikawa, M. Kinjo, and Y. Ohsumi. 2012. Atg9 vesicles are an important membrane source during early steps of autophagosome formation. *J. Cell Biol.* 198:219–233. https://doi.org/10.1083/jcb.201202061

Supplemental material

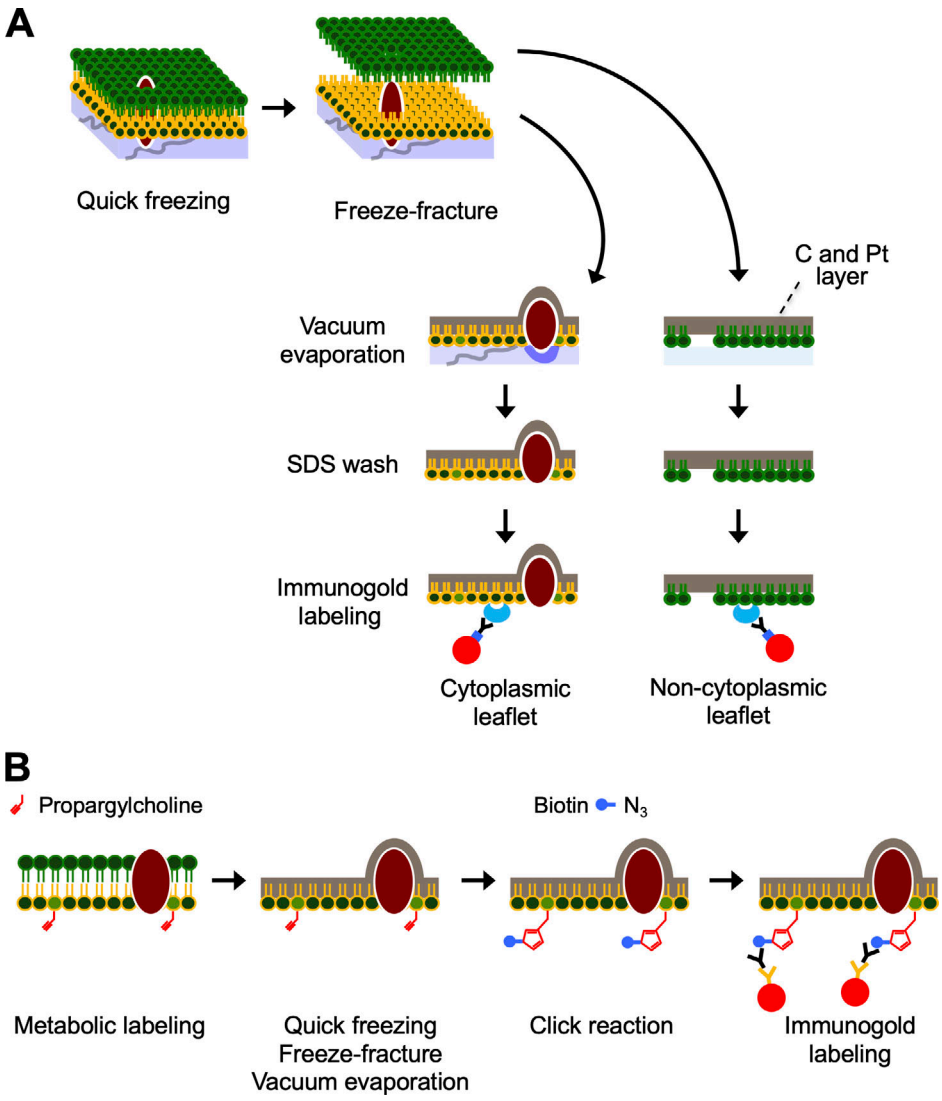

Figure S1. **The outline of freeze-fracture replica labeling. (A)** Conventional QF-FRL. The samples (e.g., live yeast cells) are quick frozen by high-pressure freezing and subjected to freeze fracture, which splits the membrane lipid bilayer into two monolayers. Thin layers of carbon and platinum are deposited onto the exposed hydrophobic side of these monolayers by vacuum evaporation. After thawing, the replicas are treated with SDS to remove nonmembranous materials and labeled with a lipid-binding protein followed by colloidal gold. **(B)** Metabolic labeling of PtdCho and click reaction on freeze-fracture replicas. Propargylcholine incorporated into the head group of PtdCho is conjugated with biotin-azide by click reaction and labeled with anti-biotin antibody and colloidal gold.

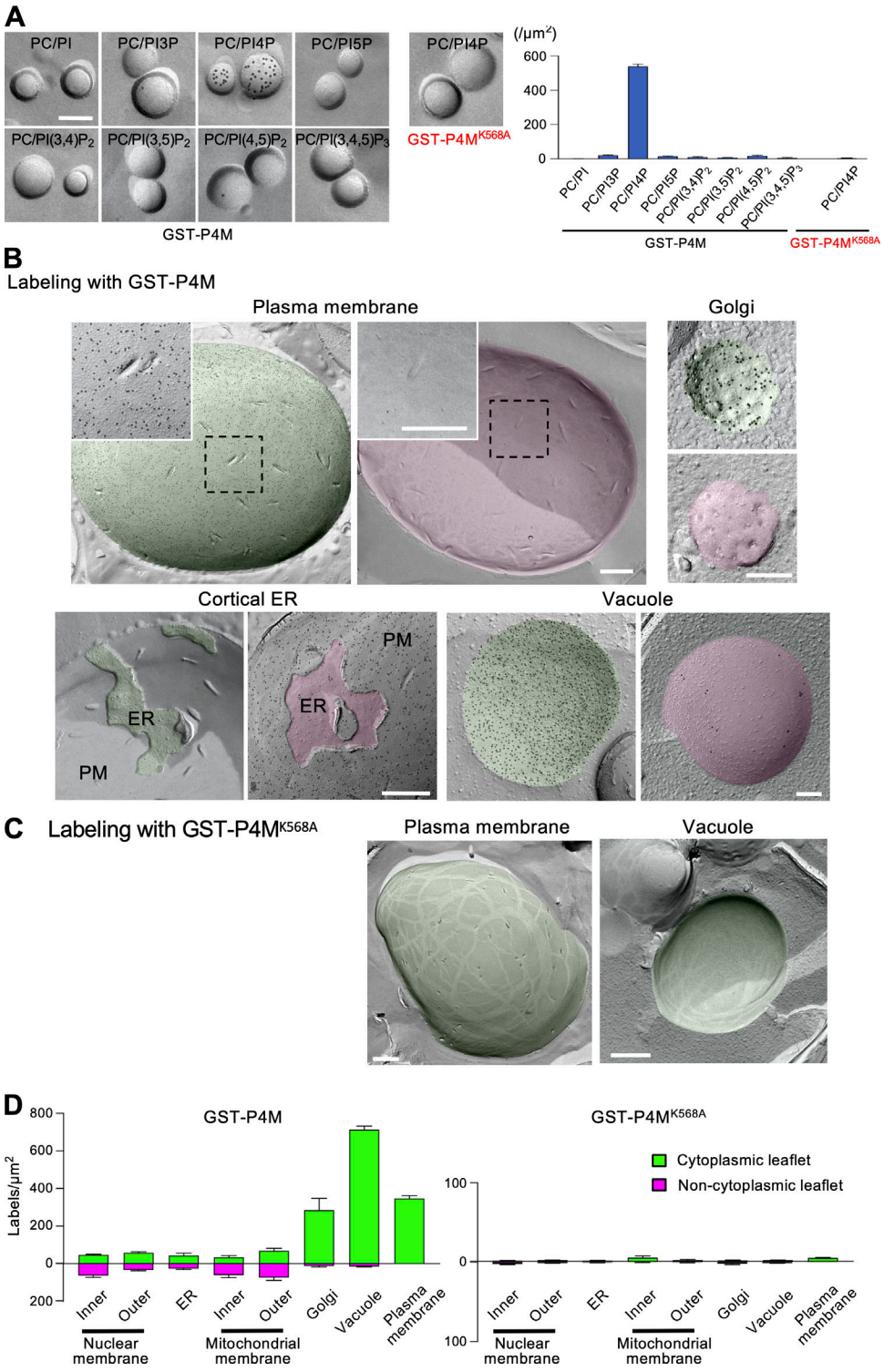

Figure S2. **Labeling of PtdIns(4)P. (A)** Liposomes prepared from 95 mol% PtdCho (PC) and 5 mol% of phosphatidylinositol (PI) or a phosphoinositide. Freeze-fracture replicas were labeled with GST-P4M or GST-P4M^{K568A}, which lacks the PtdIns(4)P binding affinity. Scale bar, 0.2 µm. The label density in liposomes (the number of gold particles/µm^2). *n* = 126 (PC/PI), 135 (PC/PI3P), 185 (PC/PI4P), 144 (PC/PI5P), 132 (PC/PI(3,4)P_2), 130 (PC/PI(3,5)P_2), 112 (PC/PI(4,5)P_2), and 120 (PC/PI(3,4,5)P_3; GST-P4M); and 122 (PC/PI4P; GST-P4M^{K568A}). A representative result of two independent experiments; mean ± SEM. **(B and C)** Labeling of yeast in normal growth condition with GST-P4M (B) or GST-P4M^{K568A} (C). The cytoplasmic and noncytoplasmic leaflets are colored green and pink, respectively. Scale bars, 0.5 µm (plasma membrane [PM]), 0.2 µm (others). **(D)** The labeling density in various membranes of yeast (the number of gold particles/µm^2). *n* = 29/33/33/30 (inner nuclear membrane), 33/33/33/32 (outer nuclear membrane), 33/33/32/29 (ER), 30/30/33/29 (inner mitochondrial membrane), 30/30/29/33 (outer mitochondrial membrane), 25/27/30/32 (Golgi), 31/32/41/31 (vacuole), and 30/30/30/32 (plasma membrane); the numbers are in the order of SidM-cytoplasmic, SidM-noncytoplasmic, SidM^{K568A}-cytoplasmic, and SidM^{K568A}-noncytoplasmic. Pooled data from three or four independent experiments; mean ± SEM.

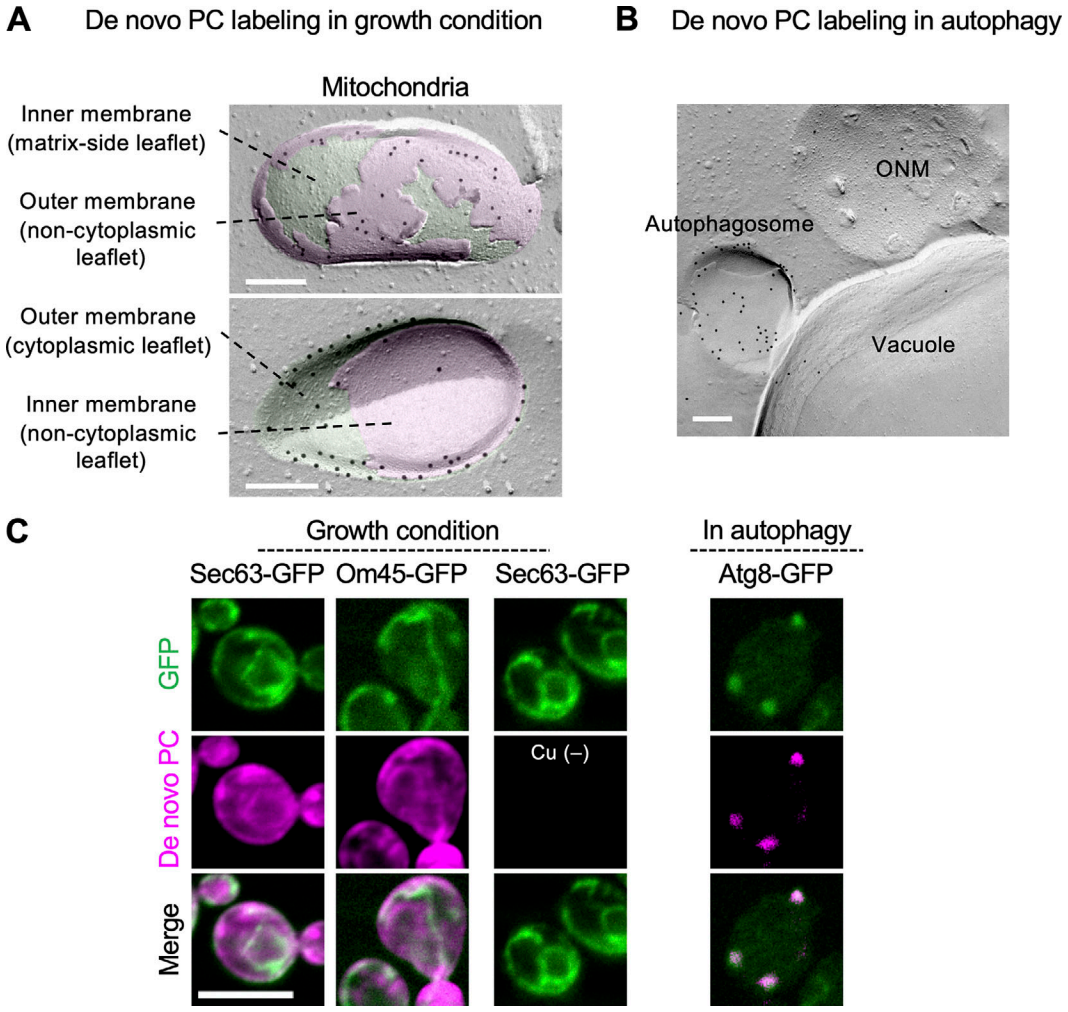

Figure S3. **Labeling of de novo–synthesized PtdCho (PC). (A)** Yeast in normal growth condition. The convex and concave fracture profiles of mitochondria are shown. The cytoplasmic and noncytoplasmic leaflets are colored green and pink, respectively. Scale bars, 0.2 µm. **(B)** Yeast cultured in S(–NC). The autophagosome, the outer nuclear membrane (ONM), and the vacuole are shown. Scale bar, 0.2 µm. **(C)** Fluorescence micrographs showing de novo–synthesized PtdCho and organelle markers. Sec63-GFP (ER), Om45-GFP (mitochondria), and Atg8-GFP (autophagosome). A negative control for the click PtdCho labeling, the omission of copper sulfate is also shown. Scale bar, 5 µm.

Table S1, provided online, lists the yeast strains used in this study.